

See discussions, stats, and author profiles for this publication at: <https://www.researchgate.net/publication/47632485>

Adsorption of Transgenic Insecticidal Cry1Ab Protein to SiO₂. 1. Forces Driving Adsorption

ARTICLE *in* ENVIRONMENTAL SCIENCE AND TECHNOLOGY · OCTOBER 2010

Impact Factor: 5.33 · DOI: 10.1021/es103008s · Source: PubMed

CITATIONS

30

READS

43

3 AUTHORS, INCLUDING:



Michael Sander

ETH Zurich

43 PUBLICATIONS 1,126 CITATIONS

SEE PROFILE

Adsorption of Transgenic Insecticidal Cry1Ab Protein to SiO₂.

1. Forces Driving Adsorption

MICHAEL SANDER,*
MICHAEL MADLIGER, AND
RENÉ P. SCHWARZENBACH

*Institute of Biogeochemistry and Pollutant Dynamics (IBP),
ETH Zurich, Zurich, Switzerland*

*Received December 8, 2009. Revised manuscript received
October 6, 2010. Accepted October 7, 2010.*

Genetically modified *Bt* crops express insecticidal Cry proteins (*Bt* toxins) that may enter agricultural soils. A mechanistic understanding of Cry protein adsorption to soils is critical for risk assessment, as this process governs Cry protein fate and bioavailability. We used quartz crystal microbalance and optical waveguide lightmode spectroscopy to elucidate the driving forces of the adsorption of monomeric Cry1Ab to negatively charged quartz (SiO₂) and positively charged poly-*L*-lysine (PLL) at pH 5–8 and constant ionic strength of 50 mM (NaCl). Bovine serum albumin and hen egg white lysozyme were used as reference proteins because of their known adsorption behavior. Electrostatics governed Cry1Ab adsorption; as pH increased above the isoelectric point of Cry1Ab, the initial rate and the extent of adsorption decreased on SiO₂ and increased on PLL. Reversible adsorption to SiO₂ suggested weak Cry1Ab–SiO₂ electrostatic interactions and no irreversible conformational changes of Cry1Ab at the surface. High conformational stability of Cry1Ab was further supported by supply rate-independent extent of adsorption of Cry1Ab to apolar gold. Some evidence is presented that the nonuniform surface charge distribution of Cry1Ab resulted in patch-controlled electrostatic attraction with sorbents that carried the same net charge as Cry1Ab. A more detailed discussion of this mechanism is given in a companion paper.

Introduction

Genetically modified *Bt* crops express one or more gene sequences from the bacterium *Bacillus thuringiensis* that code for insecticidal Cry proteins (*Bt* toxins), which provide protection against specific pest insects. Since their market introduction in 1996, *Bt* crops became an integral component of pest management practices in many countries. *Bt* maize is the second most common transgenic crop, grown on ~42 million hectares, worldwide, in 2009 (1). By various pathways, Cry proteins may be released to soils, where they have been detected in the $\mu\text{g kg}^{-1}$ range (2, 3). Some Cry proteins were shown to persist in soil for months following harvest and some to remain insecticidal in soils (2–6). Concern has been raised that Cry proteins in soils may accumulate over time and adversely affect nontarget soil-dwelling organisms (6). Assessing these risks requires that the processes governing the fate of Cry proteins in soils, most importantly the adsorption to mineral and organic soil surfaces, are under-

stood. Adsorption affects protein mobility, bioavailability, degradability, and, hence, persistence and accumulation. Desorption of adsorbed Cry proteins upon changes in solution chemistry may result in spatially and temporally high pore water Cry protein concentrations.

Previous studies have investigated adsorption of Cry proteins to clay minerals, iron- and aluminum (hydr-)oxides, silica, mica, humic acids, and natural soils (e.g. refs 7–12). A molecular level picture of Cry protein adsorption, however, is missing. Advancing this picture requires experiments in which purified proteins are used, the solution pH and ionic strength (*I*) are properly controlled, and adsorbed protein is directly quantified on the sorbent surface (and not indirectly via solution depletion). None of the previous studies has met all of these requirements.

The goal of the work presented in this and a companion paper (13) was to identify the major driving force(s) for Cry protein adsorption to charged, polar surfaces. Electrostatic and van der Waals (vdW) interactions play a major role in the interaction of proteins with such surfaces (14), while the hydrophobic effect is considered less important. If adsorbed proteins undergo conformational changes on the sorbent surface, these changes result in a gain in protein conformational entropy (14), which additionally drives adsorption. Interfacial conformational changes also increase the number of protein segments that interact with the sorbent surface and, hence, the activation free energy for desorption, leading to irreversible adsorption. For proteins with low interfacial conformational stabilities, this driving force may lead to adsorption even when protein–sorbent electrostatic interactions are repulsive. The conformational stability of Cry proteins and hence the significance of this process in the adsorption of Cry proteins is unknown.

In this paper, we discuss the relative importance of electrostatic interactions, vdW interactions, and conformational changes in the adsorption of Cry1Ab to charged polar surfaces at a constant ionic strength (*I* = 50 mM). Cry1Ab is expressed by several commercially important *Bt* maize events and served as a model Cry1A protein. The net surface charge of Cry1Ab changes from positive at pH 5 to negative at pH 7 and 8. Cry1Ab, however, has a nonuniform surface charge distribution (Table 1). Cry1Ab adsorption was compared to adsorption of two well-studied reference proteins, bovine serum albumin (BSA) and hen egg white lysozyme (HEWL) that have different surface net charges and conformational stabilities (Table 1). Quartz (SiO₂) and poly-*L*-lysine (PLL) polymeric films served as model surfaces, which were negatively and positively charged over the tested pH range, respectively. To assess the relative Cry1Ab conformational stability, proteins were also adsorbed to an apolar gold surface at pH 6.

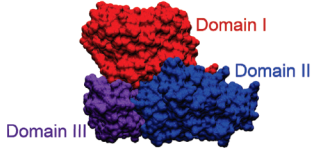
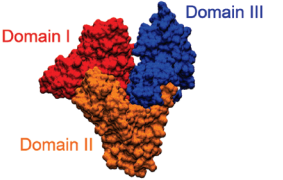
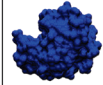
Adsorption was studied by a combination of two *in situ* surface techniques, quartz crystal microbalance with dissipation monitoring (QCM-D), the primary technique, and optical waveguide lightmode spectroscopy (OWLS). Both techniques allow direct and label-free quantification of the kinetics, extents, and reversibility of protein adsorption. QCM-D senses the “wet” mass of adsorbed proteins (i.e., adsorbed protein plus protein-associated water), whereas OWLS senses only the absolute (“dry”) adsorbed protein mass. These techniques have previously been combined to characterize protein adsorption (15).

Experimental Section

Proteins and Chemicals. Cry1Ab (provided by M. Pusztai-Carey, Case Western Reserve University, Cleveland, OH, USA)

* Corresponding author phone: 0041-(0)44 6328314; fax: 0041-(0)44 6331122; e-mail: michael.sander@env.ethz.ch.

TABLE 1. Physicochemical Properties of Transgenic Cry1Ab Protein and Reference Proteins Bovine Serum Albumin and Hen Egg White Lysozyme

| | Cry1Ab | | | | Bovine serum albumin (BSA) | | | | Hen egg white lysozyme (HEWL) | |
|--------------------------------|---|------------------|------------------|------------------|--|------------------|------------------|------------------|---|--|
| molecular weight | 66.6 kDa ^a | | | | 66.4 kDa ^a | | | | 14.3 kDa ^a | |
| molecular shape and size | Elongated ^b 7.6×6.2×5.0 nm ^b | | | | Heart shaped ^b Side length: 7.5 nm; thickness: 5 nm ^b | | | | Ellipsoid ^b 4.2×3.0×3.0 nm ^b | |
| |  | | | |  | | | |  | |
| conformational stability | unknown | | | | low ^c | | | | high ^c | |
| isoelectric point | total | domain I | domain II | domain III | total | domain I | domain II | domain III | total | |
| | 6.0 ^d (6.4 ^e) | 4.7 ^e | 9.4 ^e | 9.6 ^e | 4.7–5.3 ^e (5.6 ^e) | 5.5 ^e | 5.3 ^e | 7.6 ^e | 11.0 ^e (10.5 ^e) | |
| diffusion coefficient <i>D</i> | 5.35 10 ⁻⁷ cm ² s ⁻¹ ^f | | | | 6.09 10 ⁻⁷ cm ² s ⁻¹ ^g | | | | 1.23 10 ⁻⁶ cm ² s ⁻¹ ^g | |

^a Based on primary sequence (section S1, Supporting Information (SI)). ^b Based on crystallography data of Cry1Aa (PDB ID: 1CIY) (16) with 88% sequence homology to Cry1Ab (section S1, SI), human serum albumin (PDB ID: 1A06) (17) with 75.6% sequence homology to BSA, and of HEWL (PDB ID: 1HEL) (18). ^c Reference 19. ^d Based on experimental IEP of Cry1Ac (20) (section S1, SI). ^e Calculated with program *Theoretical pI/M_w*, ExPASy Proteomics tools. ^f Estimated by the Stokes–Einstein relation using an averaged measured hydrodynamic radius (*r_h* = 4 nm) of monomeric Cry1Aa (8) (section S1, SI). ^g Reference 21.

was extracted from protoxin from *Bacillus thuringiensis* subsp. *kurstaki* HD-1, expressed as a single gene product in *E. coli*, activated, purified, and lyophilized (details in section S1, Supporting Information (SI)). High purity HEWL and BSA (>99%, lyophilized) were from Fluka and Sigma, respectively, and used as received. The physicochemical properties of Cry1Ab, HEWL, and BSA are given in Table 1. The preparation of protein solutions and of Cry1Ab quantification is described in section S2 (SI). All chemicals used were analytical grade (section S1, SI).

Sorbents. SiO₂-coated QCM-D sensors (QXS303; Q-Sense) and SiO₂-coated OWLS waveguides (OW2400 sensor chips; Microvacuum Ltd., Budapest, Hungary; sputter coated with a 12 nm silicon oxide (SiO₂) layer in a Laybold DC-magnetron Z600 sputtering unit (Paul Scherrer Institute, Villigen, Switzerland)) were used as model quartz surfaces (isoelectric point IEP_{SiO₂} ≈ 2–3). For adsorption to PLL, sensors were coated by running solutions containing 100 mg_{PLL} L⁻¹ over the SiO₂-sensors for 30 min, resulting in fast, electrostatically driven irreversible adsorption of thin PLL films (IEP_{PLL} = 9.0–9.8 (22)) (Tables S1, S2; SI). PLL-coated sensors were rinsed with PLL-free solutions prior to switching to protein-containing solutions. Gold-coated QCM-D sensors (type QXS301) served as a model apolar sorbent. All sensors and waveguides were thoroughly cleaned before use (section S3; SI).

QCM-D measurements were conducted on a Q-Sense E4 system (Q-Sense AB, Gothenburg, Sweden) with four laminar slit shear flowcells, each containing a piezoelectric quartz crystal sensor. QCM-D monitors shifts in the resonance frequency (*f* = 5 MHz) and its overtones (*n*) as well as the dissipation (*D*) of the sensor upon adsorption/desorption of a viscoelastic protein film to its surface (23). For thin and rigid protein films, the total sensed “wet” mass ($\Delta m_{\text{QCM-D}}$ (ng cm⁻²), the sum of the masses of adsorbed protein, $\Delta m_{\text{protein}}$ (ng cm⁻²), and of protein-associated water, Δm_{water} (ng cm⁻²) is proportional to $-\Delta f_n$ (Hz) according to the Sauerbrey relation (23)

$$\Delta m_{\text{QCM-D}} = \Delta m_{\text{protein}} + \Delta m_{\text{water}} = C \cdot \frac{-\Delta f_n}{n} \quad (1)$$

where C (= 17.7 ng Hz⁻¹ cm⁻²) is the mass sensitivity constant. In most systems, normalization to $n = 3$ to 11 resulted in overlapping frequency curves and the investigated films showed small dissipation values ΔD , such that eq 1 was valid. All reported $\Delta m_{\text{QCM-D}}$ were calculated from $n = 5$ (25 MHz).

OWLS measurements were conducted on an OWLS 110 instrument (Microvacuum Ltd., Budapest, Hungary). Solutions were run through a laminar slit shear flowcell over a planar waveguide. An optical grating at the waveguide–water interface couples a He–Ne laser into the waveguide. Adsorption of proteins to the interface changes the phase shifts of the transverse electric and transverse magnetic polarization modes of the laser (24). Assuming an optically uniform adsorbed layer, the mass of adsorbed protein, Δm_{OWLS} , is given as

$$\Delta m_{\text{OWLS}} = d_{\text{adlayer}} \cdot \frac{n_{\text{adlayer}} - n_{\text{solution}}}{dn_{\text{protein}}/dc_{\text{protein}}} \quad (2)$$

where d_{adlayer} and n_{adlayer} are the thickness and the refractive index of the adsorbed protein layer, respectively, and are simultaneously determined from the two measured phase shifts; $dn_{\text{protein}}/dc_{\text{protein}}$ is the refractive index increment of proteins (0.182 g/cm³ (25)), and n_{solution} is the refractive index of the pH buffer solutions (1.3336; pH 5 to 8, *I* = 50 mM, 20 °C measured with a refractometer (Model J357, Rudolph Research Analytical, Hackettstown, NJ, USA)). In contrast to $\Delta m_{\text{QCM-D}}$, Δm_{OWLS} corresponds only to the absolute (“dry”) mass of adsorbed proteins.

A typical adsorption experiment comprised three successive steps (Figure S5, SI): (i) Baseline generation: pH- and *I*-adjusted solutions (pH 5 ± 0.05 (3 mM acetate), pH 6 ± 0.05 (3 mM 2-(*N*-morpholino)-ethane-sulfonic acid), pH 7 ± 0.05 and pH 8 ± 0.05 (both 3 mM 4-(2-hydroxyethyl)-1-piperazine-ethanesulfonic acid); total *I* = 50 mM, adjusted

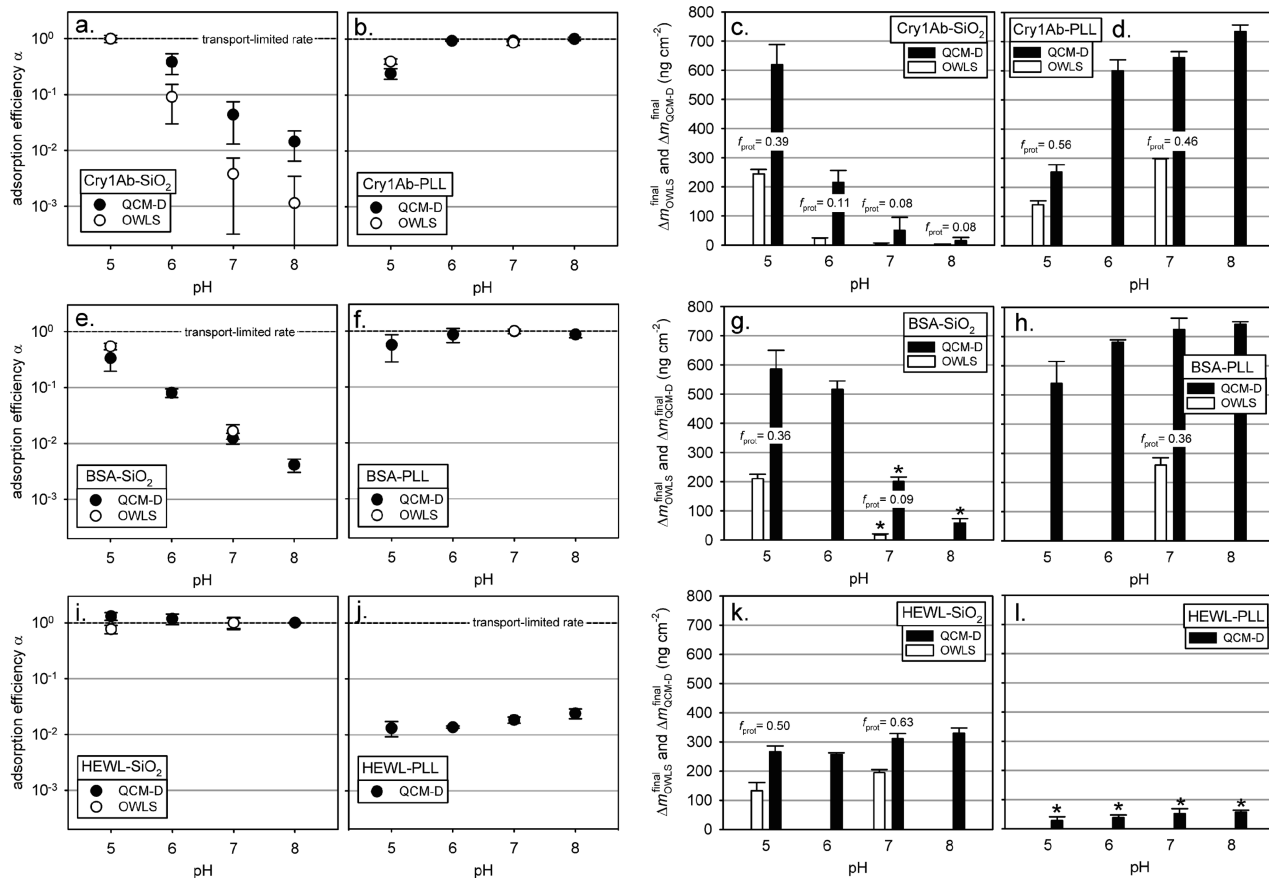


FIGURE 1. Protein adsorption efficiencies α (measured by quartz crystal microbalance with dissipation monitoring (QCM-D; filled circles) and optical waveguide lightmode spectroscopy (OWLS; open circles), and final “wet” ($\Delta m_{\text{QCM-D}}^{\text{final}}$) and “dry” ($\Delta m_{\text{OWLS}}^{\text{final}}$) adsorbed protein masses (measured by QCM-D (solid bars) and OWLS (open bars) at which adsorption plateaued, or, for systems in which protein adsorption did not plateau, at which rinsing was initiated (marked by asterisk (*)). f_{prot} is the fraction of “dry” adsorbed protein mass to the total adsorbed “wet” mass (i.e., $f_{\text{prot}} = (\Delta m_{\text{OWLS}}^{\text{final}})/(\Delta m_{\text{QCM-D}}^{\text{final}})$). The error bars represent standard deviations of replicate measurements. a–d: Cry1Ab; e–h: reference protein bovine serum albumin (BSA); i–l: reference protein hen egg white lysozyme (HEWL); a, c, e, g, i, k: sorbent: negatively charged quartz (SiO_2); b, d, f, h, j, l: sorbent: positively charged poly-L-lysine (PLL).

by NaCl) were pumped with a peristaltic pump over the sensors/waveguides until the signal baseline remained stable. (ii) Adsorption: Protein-containing solutions ($1\text{--}10\ \mu\text{g protein mL}^{-1}$) of the same pH and I were run over the sensors/waveguides. Protein adsorption in most systems plateaued at a final adsorbed mass. (iii) Rinsing: The systems were rinsed with protein-free solutions of the same pH and I to study adsorption reversibility. All experiments were carried out at $20.0 \pm 0.1\ ^\circ\text{C}$ and at least in duplicates.

Adsorption data were analyzed for initial protein adsorption rates k_{ads} ($\text{ng cm}^{-2}\ \text{min}^{-1}$), final adsorbed masses $\Delta m_{\text{QCM-D}}^{\text{final}}$ and $\Delta m_{\text{OWLS}}^{\text{final}}$ (ng cm^{-2}), and for adsorption reversibility (Figure S5). k_{ads} between QCM-D and OWLS measurements and between different protein-sorbent systems were compared on the basis of the dimensionless adsorption efficiency (α)

$$\alpha = \frac{k_{\text{ads}}}{k_{\text{ads}}^{\text{max}}} \quad (3)$$

where $k_{\text{ads}}^{\text{max}}$ ($\text{ng cm}^{-2}\ \text{min}^{-1}$) is the maximum possible, transport-limited adsorption rate (i.e., no energy barrier to adsorption). While theoretical $k_{\text{ads}}^{\text{max}}$ were calculated for the OWLS system (section S4, SI), the more complex flow pattern in the QCM-D cell did not allow calculation of corresponding $k_{\text{ads}}^{\text{max}}$. α describes the fraction of protein-sorbent encounters

that result in adsorption relative to transport-limited adsorption in the absence of an energy barrier to adsorption ($\alpha = 1$).

Results and Discussion

Representative QCM-D and OWLS plots for the adsorption of Cry1Ab, BSA, and HEWL to SiO_2 and PLL at pH 5 to pH 8 are provided in Figures S6 and S7 (section S4, SI). The results of all replicate measurements are given in Tables S1 and S2 (section S4, SI).

Transport-Limited Protein Adsorption Rates. In the OWLS setup, the highest initial adsorption rates k_{ads} ($43.8 \pm 1.7\ \text{ng cm}^{-2}\ \text{min}^{-1}$) of Cry1Ab to SiO_2 were measured at pH 5. These rates agreed very well with the calculated transport-limited initial adsorption rate $k_{\text{ads}}^{\text{max}}$ for monomeric Cry1Ab ($46.7\ \text{ng cm}^{-2}\ \text{min}^{-1}$; section S4, SI). Similarly, the highest k_{ads} found for the adsorption of BSA to PLL ($48.0 \pm 1.2\ \text{ng cm}^{-2}\ \text{min}^{-1}$) and HEWL to SiO_2 ($83.2 \pm 20.3\ \text{ng cm}^{-2}\ \text{min}^{-1}$) at pH 7 agreed well with the respective $k_{\text{ads}}^{\text{max}}$ of the monomeric proteins (50.9 and $81.4\ \text{ng cm}^{-2}\ \text{min}^{-1}$, respectively; section S4, SI). These findings indicate that the initial adsorption rates in these protein-sorbent systems were transport limited. We therefore used these initial adsorption rates, measured by OWLS and QCM-D, as $k_{\text{ads}}^{\text{max}}$ to calculate α from the OWLS and QCM-D measured k_{ads} , respectively (eq 3).

Adsorption Efficiencies and Final Adsorbed Amounts. Figure 1 shows the adsorption efficiencies (α) as a function

of pH for all protein-sorbent systems and the corresponding final adsorbed mass on the QCM-D ($\Delta m_{\text{QCM-D}}^{\text{final}}$) and OWLS ($\Delta m_{\text{OWLS}}^{\text{final}}$), which was quantified when adsorption plateaued or, for protein-sorbent systems in which adsorption did not plateau during the adsorption period, when rinsing was initiated.

Comparison of QCM-D and OWLS. Overall, α values determined by QCM-D and OWLS showed good quantitative agreement in all protein-sorbent systems, except for Cry1Ab adsorption to SiO₂ at pH ≥ 6 , for which α values showed the same pH trends but were larger for QCM-D than OWLS measurements. Furthermore, the α values in the Cry1Ab-SiO₂ system at pH ≥ 6 showed the largest uncertainties among all tested systems. As subsequently discussed, these findings reflect the relatively weak Cry1Ab-SiO₂ interactions and were, at least in part, ascribable to slight physicochemical differences in the SiO₂ surfaces of the QCM-D sensors and OWLS waveguides.

QCM-D and OWLS yielded consistent trends of $\Delta m_{\text{QCM-D}}^{\text{final}}$ and $\Delta m_{\text{OWLS}}^{\text{final}}$ with pH and sorbent net charge, while, as expected, $\Delta m_{\text{QCM-D}}^{\text{final}}$ were always larger than $\Delta m_{\text{OWLS}}^{\text{final}}$, because QCM-D senses protein-associated water. Changes in pH that affected protein-sorbent affinities were consistently reflected in both the magnitude of initial kinetics (α) and in the final extent of protein adsorption ($\Delta m_{\text{QCM-D}}^{\text{final}}$ and $\Delta m_{\text{OWLS}}^{\text{final}}$). For the sake of brevity, discussion of $\Delta m_{\text{QCM-D}}^{\text{final}}$ and $\Delta m_{\text{OWLS}}^{\text{final}}$ will subsequently be denoted by Δm^{final} . The exact values of α and Δm^{final} are provided in Tables S1 and S2 (SI).

For Cry1Ab adsorption to SiO₂, α decreased with increasing pH from $\alpha \approx 1$ at pH 5 to $\alpha < 0.02$ at pH 8 (Figure 1a). Hence, 50 times as many Cry-SiO₂ encounters were required at pH 8 to result in one adsorption event as compared to the transport-limited adsorption rates. Compared to SiO₂, adsorption to positively charged PLL showed the opposite pH-dependence (Figure 1b) of α , with $\alpha \approx 0.24$ at pH 5 and $\alpha \approx 1$ at pH 6–8.

The finding of $\alpha \approx 1$ of Cry1Ab to SiO₂ at pH 5 and to PLL at pH 6–8 implies that Cry1Ab was monomeric at all tested pH. The decrease in α to SiO₂ with increasing pH can, therefore, be rationalized by decreasing affinities of the monomeric Cry1Ab to SiO₂. The finding of monomeric Cry1Ab stands in contrast to refs 8 and 12, which reported that Cry1Aa formed oligomers composed of more than ten monomers at $I < 150$ mM and circumneutral pH. Cry1Ab oligomers of that size would have resulted in $k_{\text{ads}}^{\text{max}} < 28$ ng cm⁻² min⁻¹ in the OWLS setup, which is much smaller than the experimental k_{ads} . Since the physicochemical properties of Cry1Aa and Cry1Ab are quite similar (88% sequence homology), they cannot be invoked to explain the apparently different tendencies of the proteins to oligomerize. Oligomerization in refs 8 and 12 may therefore have resulted primarily from the use of up to 100-fold higher Cry1Aa concentrations as compared to the Cry1Ab concentrations used in this study.

Consistent with the pH trends of α , with increasing pH, Δm^{final} of Cry1Ab decreased to SiO₂, while it increased to PLL (Figure 1c,d). The inversed pH trends on the oppositely charged sorbents strongly suggest that Cry1Ab-sorbent electrostatic interactions played a major role in adsorption. Increasing the negative surface charge of Cry1Ab with increasing pH resulted in decreasing Cry1Ab-SiO₂ electrostatic attraction and in increasing electrostatic attraction in the Cry1Ab-PLL system.

BSA served as a reference protein with a low conformational stability and with a similar molecular size and IEP as Cry1Ab (Table 1). Electrostatic repulsion of BSA from like-charged SiO₂ explains, at least in part, the decrease in α and Δm^{final} of BSA to SiO₂ with increasing pH (Figure 1e,g). Previous work has shown that significant BSA adsorption to SiO₂ at pH $> \text{IEP}_{\text{BSA}}$ despite electrostatic repulsion was due

to interfacial conformational changes of BSA (26, 27). Similar to Cry1Ab, initial adsorption rates of BSA to PLL were transport-limited at pH 6 to 8, and adsorption was extensive (Figure 1f,h), reflecting electrostatic attraction of net negatively charged BSA to positively charged PLL.

In contrast to BSA, HEWL has a high conformational stability and, in contrast to Cry1Ab, a uniform surface charge distribution. Therefore, changes in the orientation of HEWL to SiO₂ only slightly modify overall strong electrostatic attraction, resulting in $\alpha \approx 1$ from pH 5–8 and in Δm^{final} values that were only slightly affected by solution pH (Figure 1i,k), which is consistent with refs 28 and 29. Conversely, all orientations of HEWL to PLL resulted in electrostatic repulsion, leading to approximately 30-fold lower α values relative to SiO₂ and resulted in slow continuous adsorption to small Δm^{final} values (Figure 1j,l). The large difference in α and Δm^{final} values between SiO₂ and PLL also provides good evidence that PLL coated most of, if not, the entire SiO₂ surface.

Monolayer Adsorption. Systems with transport-limited adsorption ($\alpha \approx 1$) plateaued at reproducible Δm^{final} (Figure 1, Tables S1, S2), which, for numerous reasons, can be assumed to correspond to protein monolayers: (i) Adsorption of Cry1Ab and BSA to PLL at pH 7 from solutions that covered a factor of 20 in the protein concentration plateaued at comparable $\Delta m_{\text{QCM-D}}^{\text{final}} \approx 620$ and 640 ng cm⁻², respectively (Figure S9, SI). Such concentration-independent maximum adsorbed masses imply that adsorption was limited by the number of adsorption sites. Furthermore, similar $\Delta m_{\text{QCM-D}}^{\text{final}}$ and $\Delta m_{\text{OWLS}}^{\text{final}}$ of Cry1Ab and BSA to SiO₂ at pH 5 and to PLL at pH 6 to 8 (Figure 1; Tables S1, S2) were consistent with comparable monolayer adsorbed masses of globular proteins with comparable sizes. Δm^{final} of HEWL were smaller due to its smaller molecular weight and hence less adsorbed mass per protein footprint. (ii) The experimental $\Delta m_{\text{QCM-D}}^{\text{final}}$ and $\Delta m_{\text{OWLS}}^{\text{final}}$ of Cry1Ab, BSA, and HEWL corresponded well to the respective theoretical “wet” and “dry” adsorbed masses of full monolayers, calculated based on the molecular dimensions of the proteins (section S5, SI). (iii) Viscoelastic modeling of the QCM-D frequency and dissipation values of several overtones resulted in an estimated adlayer thickness of ~ 6 – 7 nm for Cry1Ab and BSA and ~ 3 nm for HEWL (section S5, SI), which corresponded well to the molecular dimensions of the proteins and, hence, monolayer adsorption. (iv) The ratios of $\Delta m_{\text{OWLS}}^{\text{final}}$ to $\Delta m_{\text{QCM-D}}^{\text{final}}$, f_{prot} , were approximately 40 to 50% (Figure 1), consistent with previously published values for the contribution of protein mass to the total QCM-D sensed mass in full protein monolayers (15, 30). Lower $f_{\text{prot}} \approx 8$ – 9% for Cry1Ab and BSA adsorption to SiO₂ at pH 7–8 are consistent with refs 15 and 30, reflecting that the mass of water that couples to each protein molecule is larger at lower sorbent surface coverage. (v) As subsequently discussed, adsorption was irreversible in all systems with $\alpha = 1$, except for Cry1Ab-SiO₂ at pH 5. Irreversible adsorption implies that adsorption plateaued as the maximum (jamming) concentration of proteins on the sorbent surface was attained, corresponding to a monolayer.

Reversibility. Adsorption in all investigated protein-sorbent systems was largely irreversible, except for Cry1Ab adsorption to SiO₂ (decrease in $\Delta m_{\text{QCM-D}}$ and Δm_{OWLS} during buffer rinsing; Figures S6 and S7). Reversible Cry1Ab-SiO₂ interactions imply (i) that adsorbed and solution phase Cry1Ab molecules were in dynamic equilibrium (adsorption plateaued because the adsorptive equaled the desorptive protein fluxes), (ii) that the sum of Cry1Ab-SiO₂ electrostatic and vdW interactions were relatively weak, and (iii) no extensive, irreversible conformational changes of adsorbed Cry1Ab, which would have resulted in adsorption irreversibility. Conversely, irreversible adsorption of BSA to SiO₂ at pH $> \text{IEP}_{\text{BSA}}$ is consistent with conformational changes of BSA on SiO₂. vdW interactions most likely did not cause

irreversible adsorption of BSA to SiO₂, as vdW interactions for the similarly sized Cry1Ab, which adsorbed reversibly, must have been comparable. The difference in Cry1Ab and BSA adsorption reversibility shows that their adsorption was governed by different driving forces despite the similar effects of pH and sorbent net charge on the kinetics and extents of Cry1Ab and BSA adsorption to SiO₂ (and PLL). Irreversible adsorption of HEWL to SiO₂ reflected strong electrostatic attraction due to the high positive surface charge density of HEWL over the investigated pH range ($\text{pH} \ll \text{IEP}_{\text{HEWL}}$).

Driving Forces for Cry1Ab Adsorption to SiO₂. The importance of electrostatic interactions of Cry1Ab with charged sorbents is apparent from the effects of pH and sorbent net charges on Cry1Ab adsorption. However, Figure 1 shows that Cry1Ab adsorbed also to like-charged SiO₂ at $\text{pH} > \text{IEP}_{\text{Cry1Ab}}$ and to like-charged PLL at $\text{pH} < \text{IEP}_{\text{Cry1Ab}}$. There are two possible explanations for Cry1Ab adsorption in these systems. The first explanation assumes that the surface net charge of Cry1Ab governed its electrostatic interactions with charged sorbents. In this case, Cry1Ab-sorbent electrostatic repulsion had to be overcompensated by additional Cry1Ab-sorbent interaction forces. The second explanation assumes that Cry1Ab was oriented with positively charged surface patches toward SiO₂ and with negatively charged patches toward PLL. Such patch-controlled electrostatic attraction is conceivable based on the nonuniform surface charge distribution of Cry1Ab (Table 1). These two alternative explanations will be subsequently evaluated.

Electrostatic repulsion may, in principle, be overcompensated by attractive vdW interactions, protein conformational changes on the sorbent, as for BSA, and the hydrophobic effect. The latter effect must play a small role in the adsorption of Cry1Ab to SiO₂ surface, due to its high polarity, as confirmed by small contact angles of water ($<5^\circ$) measured on the SiO₂ sensors. vdW interactions unlikely overcompensated Cry1Ab-SiO₂ electrostatic repulsion at $\text{pH} > \text{IEP}_{\text{Cry1Ab}}$, because previous work has demonstrated that electrostatic interactions predominate over vdW interactions at $I < 100$ mM, even for moderately charged proteins (31). Furthermore, weaker vdW interactions are expected between Cry1Ab and PLL (a water-rich film with low Hamaker constant) than between Cry1Ab and SiO₂ (larger Hamaker constant as compared to PLL). vdW interactions, therefore, cannot explain why Cry1Ab adsorption was irreversible to PLL but reversible to SiO₂.

Reversible Cry1Ab-SiO₂ interactions suggest that Cry1Ab did not undergo extensive conformational changes on SiO₂ (see above discussion). To further assess the conformational stability of Cry1Ab, we studied the effect of protein supply rate on $\Delta m_{\text{QCM-D}}^{\text{final}}$ of all three proteins on gold-coated QCM-D sensors. Different supply rates were obtained by using different protein concentrations ($2\text{--}20\ \mu\text{g mL}^{-1}$) at a constant volumetric flow rate (and hence wall shear rate). Gold was chosen as apolar surfaces induce larger conformational changes in adsorbed proteins than polar surfaces (32). Proteins with low conformational stability are expected to show decreasing $\Delta m_{\text{QCM-D}}^{\text{final}}$ with decreasing supply rates. At low supply rates, adsorbed proteins have more time to undergo time-dependent interfacial spreading before adjacent sites become occupied by other protein molecules, resulting in larger protein footprints on the sorbent surface and, hence, a smaller number of proteins adsorbed in a unit area of the sorbent (32, 33).

Figure 2 shows $\Delta m_{\text{QCM-D}}^{\text{final}}$ versus the product of the protein bulk concentration, c_{protein} , and time t . This approach to normalize different protein concentrations is justified because the volumetric flow rates, and hence the shear rates, were constant in each sorbent-protein system. Constant shear rates are also apparent from k_{ads} that scaled linearly with the bulk protein concentration for all proteins (inserts in Figure

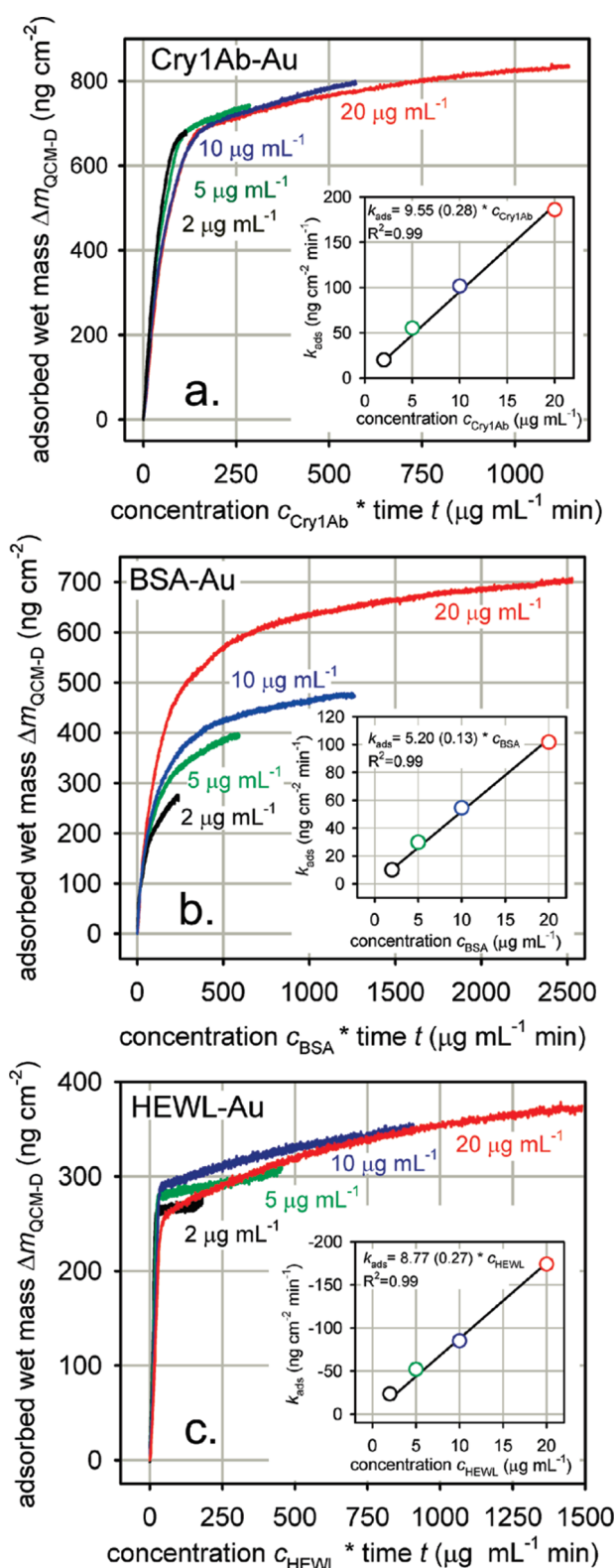


FIGURE 2. Adsorbed “wet” protein mass $\Delta m_{\text{QCM-D}}$ on gold-coated QCM-D sensors versus the bulk protein concentration $c_{\text{protein}} * \text{time } t$ ($\text{pH } 6$, $I = 50$ mM). a. Cry1Ab b. bovine serum albumin (BSA), and c. hen egg white lysozyme (HEWL). Inserted graphs: Initial adsorption rates k_{ads} versus c_{protein} . The chosen normalization is applicable as the volumetric flow rates Q , and therefore the wall shear rates were constant within each set of experiment ($Q = 100\ \mu\text{L min}^{-1}$ for Cry1Ab and BSA and $Q = 50\ \mu\text{L min}^{-1}$ for HEWL (section S4, SI)).

2), which, however, had different effects on $\Delta m_{\text{QCM-D}}^{\text{final}}$ for the three proteins. For Cry1Ab and HEWL, the concentration-normalized $\Delta m_{\text{QCM-D}}$ overlapped and started to plateau at very similar values. These findings strongly suggest that Cry1Ab and HEWL did not undergo slow kinetic spreading on the surface, consistent for HEWL with its high conformational stability (19, 28). Conversely, the $\Delta m_{\text{QCM-D}}^{\text{final}}$ of BSA markedly decreased with decreasing supply rates, implying extensive time-dependent interfacial spreading. The noted irreversible adsorption ruled out that decreasing $\Delta m_{\text{QCM-D}}^{\text{final}}$ with decreasing BSA concentrations resulted from concentration-dependent dynamic equilibria between Au-adsorbed and solution phase BSA molecules. These findings clearly suggest that Cry1Ab has a conformational stability much higher than that of BSA and comparable to that of HEWL. The absence of extensive conformational changes of Cry1Ab on the apolar Au surface strongly suggests conformational stability of Cry1Ab on the more polar SiO₂ and, hence, that conformational changes did not drive Cry1Ab adsorption to SiO₂ at pH > IEP_{Cry1Ab}.

The preceding discussion gives credence to the second explanation for Cry1Ab adsorption to surfaces of the same net charge as the protein: patch-controlled electrostatic attraction, by which Cry1Ab was oriented with positively charged patches, likely on high-IEP domains II and III, toward SiO₂ and with negatively charged patches, likely on low-IEP domain I, toward PLL (Table 1). This mechanism provides a plausible explanation for reversible adsorption of Cry1Ab to SiO₂ and irreversible adsorption to PLL as the acidic amino acids on domain I are concentrated on a relatively small surface patch with a high charge density (13, 16), while the basic amino acids in domains II and III are widely distributed over the domain surfaces, resulting in a lower positive surface charge density. The patch controlled-adsorption mechanism is validated in the companion paper (13), in which we report, among other findings, the effect of ionic strength on the interactions of Cry1Ab with SiO₂ and PLL.

Implications

This study demonstrates (i) that electrostatic interactions govern the adsorption of monomeric Cry1Ab to charged, polar surfaces, (ii) that the sum of electrostatic and vdW interaction of Cry1Ab to negatively charged surfaces is weak at pH > 5 and $I = 50$ mM, resulting in reversible adsorption, and (iii) that Cry1Ab has a high interfacial conformational stability. These findings have several implications. First, we expect that the adsorption of Cry1Ab to charged mineral oxide/hydroxide surfaces in soils, including Fe- and Al-(hydr)oxides and clay minerals, are also governed by electrostatic interactions. Weak interactions with negatively charged, polar (mineral) surfaces at pH > 5 are likely to result in reversible, concentration-dependent adsorption. For the assessment of fate, this finding means that adsorbed Cry1Ab proteins will desorb and, hence, be mobilized upon decreasing the solution protein concentration or increasing the solution pH. Third, the high Cry1Ab conformational stability rules out rapid inactivation of adsorbed Cry1Ab in soils due to irreversible loss of its bioactive structure. In fact, the high conformational stability provides a plausible explanation for earlier findings that Cry proteins in soils remain insecticidal (4–6).

In a companion paper (13), we provide a detailed analysis of the effects of Cry1Ab concentration and solution ionic strength on Cry1Ab adsorption to SiO₂ and PLL. Forthcoming papers will address the interaction of Cry1Ab with SiO₂ particles and with humic acid films, as models for soil organic matter.

Acknowledgments

We thank the Swiss National Science Foundation, National Research Program 59 (Project 405940-115662) for funding,

Marianne P. Carey for Cry1Ab, Christoph Moschet for experimental support, and Jeanne E. Tomaszewski, Joel A. Pedersen, Kurt H. Jacobson, Kartic Kumar, Thomas B. Hofstetter, Christopher Gorski, Orane Guillaume-Gentil, and Janos Voros for helpful discussions.

Supporting Information Available

Additional data on the physicochemical properties of the proteins, the experimental procedures, raw QCM-D and OWLS adsorption measurements, estimated film thicknesses, and model calculations (transport limited adsorption rates and monolayer adsorbed masses). This material is available free of charge via the Internet at <http://pubs.acs.org>.

Literature Cited

- James, C. *Global Status of Commercialized Biotech/GM Crops: 2009*. ISAAA Brief No. 41. ISAAA: Ithaca, NY, 2009.
- Baumgarte, S.; Tebbe, C. C. Field studies on the environmental fate of the Cry1Ab Bt-toxin produced by transgenic maize (MON810) and its effect on bacterial communities in the maize rhizosphere. *Mol. Ecol.* **2005**, *14* (8), 2539–2551.
- Hopkins, D. W.; Gregorich, E. G. Detection and decay of the Bt endotoxin in soil from a field trial with genetically modified maize. *Eur. J. Soil Sci.* **2003**, *54* (4), 793–800.
- Sims, S. R.; Ream, J. E. Soil inactivation of the *Bacillus thuringiensis* subsp. *kurstaki* CryIIA insecticidal protein within transgenic cotton tissue: Laboratory microcosm and field studies. *J. Agric. Food Chem.* **1997**, *45* (4), 1502–1505.
- Crecchio, C.; Stotzky, G. Biodegradation and insecticidal activity of the toxin from *Bacillus thuringiensis* subsp. *kurstaki* bound on complexes of montmorillonite-humic acids-Al hydroxypolymers. *Soil Biol. Biochem.* **2001**, *33* (4–5), 573–581.
- Tapp, H.; Stotzky, G. Persistence of the insecticidal toxin from *Bacillus thuringiensis* subsp. *kurstaki* in soil. *Soil Biol. Biochem.* **1998**, *30* (4), 471–476.
- Pagel-Wieder, S.; Niemeyer, J.; Fischer, W. R.; Gessler, F. Effects of physical and chemical properties of soils on adsorption of the insecticidal protein (Cry1Ab) from *Bacillus thuringiensis* at Cry1Ab protein concentrations relevant for experimental field sites. *Soil Biol. Biochem.* **2007**, *39* (12), 3034–3042.
- Helassa, N.; Quiquampoix, H.; Noinville, S.; Szponarski, W.; Staunton, S. Adsorption and desorption of monomeric Bt (*Bacillus thuringiensis*) Cry1Aa toxin on montmorillonite and kaolinite. *Soil Biol. Biochem.* **2009**, *41*, 498–504.
- Crecchio, C.; Stotzky, G. Insecticidal activity and biodegradation of the toxin from *Bacillus thuringiensis* subsp. *kurstaki* bound to humic acids from soil. *Soil Biol. Biochem.* **1998**, *30* (4), 463–470.
- Chevallier, T.; Muchaonyerwa, P.; Chenu, C. Microbial utilisation of two proteins adsorbed to a vertisol clay fraction: toxin from *Bacillus thuringiensis* subsp. *tenebrionis* and bovine serum albumin. *Soil Biol. Biochem.* **2003**, *35* (9), 1211–1218.
- Muchaonyerwa, P.; Chevallier, T.; Pantani, O. L.; Nyamugafata, P.; Mpepereki, S.; Chenu, C. Adsorption of the pesticidal toxin from *Bacillus thuringiensis* subsp. *tenebrionis* on tropical soils and their particle-size fractions. *Geoderma* **2006**, *133* (3–4), 244–257.
- Janot, J.-M.; Boissière, M.; Thami, T.; Tronel-Peyroz, E.; Helassa, N.; Noinville, S.; Quiquampoix, H.; Staunton, S.; Déjardin, P. Adsorption of Alexa-labeled Bt toxin on mica, glass, and hydrophobized glass: study by normal scanning confocal fluorescence. *Biomacromolecules* **2010**, *11* (6), 1661–1666.
- Madliger, M.; Sander, M.; Schwarzenbach, R. P.; Adsorption of transgenic insecticidal Cry1Ab protein to SiO₂. 2. Patch-controlled electrostatic attraction. *Environ. Sci. Technol.*, in press, doi:10.1021/es103007u.
- Kleijn, M.; Norde, W. The adsorption of proteins from aqueous solution on solid surfaces. *Heterogen. Chem. Rev.* **1995**, *2* (3), 157–172.
- Vörös, J. The density and refractive index of adsorbing protein layers. *Biophys. J.* **2004**, *87* (1), 553–561.
- Grochulski, P.; Masson, L.; Borisova, S.; Pusztai-carey, M.; Schwartz, J. L.; Brousseau, R.; Cygler, M. *Bacillus thuringiensis* CryIA(a) insecticidal toxin: crystal structure and channel formation. *J. Mol. Biol.* **1995**, *254* (3), 447–464.
- Sugio, S.; Kashima, A.; Mochizuki, S.; Noda, M.; Kobayashi, K. Crystal structure of human serum albumin at 2.5 Å resolution. *Protein Eng.* **1999**, *12* (6), 439–446.

- (18) Wilson, K. P.; Malcolm, B. A.; Matthews, B. W. Structural and thermodynamic analysis of compensating mutations within the core of chicken egg-white lysozyme. *J. Biol. Chem.* **1992**, *267* (15), 10842–10849.
- (19) Norde, W.; Favier, J. P. Structure of adsorbed and desorbed proteins. *Colloids Surf.* **1992**, *64* (1), 87–93.
- (20) Bietlot, H.; Carey, P. R.; Choma, C.; Kaplan, H.; Lessard, T.; Pozsgay, M. Facile preparation and characterization of the toxin from *Bacillus thuringiensis* var *Kurstaki*. *Biochem. J.* **1989**, *260* (1), 87–91.
- (21) Gaigalas, A. K.; Hubbard, J. B.; McCurley, M.; Woo, S. Diffusion of bovine serum albumin in aqueous solutions. *J. Phys. Chem.* **1992**, *96* (5), 2355–2359.
- (22) Fasman, G. D. *Handbook of biochemistry and molecular biology*; CRC Press: Boca Raton, 1976.
- (23) Rodahl, M.; Höök, F.; Krozer, A.; Brzezinski, P.; Kasemo, B. Quartz crystal microbalance setup for frequency and Q-factor measurements in gaseous and liquid environments. *Rev. Sci. Instrum.* **1995**, *66* (7), 3924–3930.
- (24) Vörös, J.; Ramsden, J. J.; Csúcs, G.; Szendro, I.; De Paul, S. M.; Textor, M.; Spencer, N. D. Optical grating coupler biosensors. *Biomaterials* **2002**, *23* (17), 3699–3710.
- (25) De Feijter, J. A.; Benjamins, J.; Veer, F. A. Ellipsometry as a tool to study the adsorption behavior of synthetic and biopolymers at the air-water interface. *Biopolymers* **1978**, *17* (7), 1759–1772.
- (26) Su, T. J.; Lu, J. R.; Thomas, R. K.; Cui, Z. F. Effect of pH on the adsorption of bovine serum albumin at the silica water interface studied by neutron reflection. *J. Phys. Chem. B* **1999**, *103* (18), 3727–3736.
- (27) McClellan, S. J.; Franses, E. I. Adsorption of bovine serum albumin at solid/aqueous interfaces. *Colloid. Surf. A* **2005**, *260* (1–3), 265–275.
- (28) Su, T. J.; Lu, J. R.; Thomas, R. K.; Cui, Z. F.; Penfold, J. The effect of solution pH on the structure of lysozyme layers adsorbed at the silica-water interface studied by neutron reflection. *Langmuir* **1998**, *14* (2), 438–445.
- (29) Su, T. J.; Lu, J. R.; Thomas, R. K.; Cui, Z. F.; Penfold, J. The adsorption of lysozyme at the silica-water interface: A neutron reflection study. *J. Colloid Interface Sci.* **1998**, *203* (2), 419–429.
- (30) Bingen, P.; Wang, G.; Steinmetz, N. F.; Rodahl, M.; Richter, R. P. Solvation effects in the quartz crystal microbalance with dissipation monitoring response to biomolecular adsorption. A phenomenological approach. *Anal. Chem.* **2008**, *80* (23), 8880–8890.
- (31) Roth, C. M.; Lenhoff, A. M. Electrostatic and van der Waals contributions to protein adsorption: computation of equilibrium constants. *Langmuir* **1993**, *9* (4), 962–972.
- (32) van der Veen, M.; Stuart, M. C.; Norde, W. Spreading of proteins and its effect on adsorption and desorption kinetics. *Colloid. Surf. B* **2007**, *54* (2), 136–142.
- (33) Wertz, C. F.; Santore, M. M. Effect of surface hydrophobicity on adsorption and relaxation kinetics of albumin and fibrinogen: Single-species and competitive behavior. *Langmuir* **2001**, *17* (10), 3006–3016.

ES103008S